Formation mechanism of the hierarchic structure in lath martensite phase in steels

Kazuhiro Iwashita[1], Yoshinori Murata[1]*, Yuhki Tsukada[1] and Toshiyuki Koyama[2]

1: *Graduate School of Engineering, Nagoya University, Japan*
2: *Graduate School of Engineering, Nagoya Institute of Technology*

*Corresponding Author: Yoshinori Murata,
Department of Materials, Physics and Energy Engineering, Graduate School of Engineering,
Nagoya University, Furo-cho, Chikusa, Nagoya 464-8603, Japan

e-mail: murata@numse.nagoya-u.ac.jp
Phone & Fax: +81 52 789 3232

Formation mechanism of the hierarchic structure in lath martensite phase

Abstract

Martensitic transformation is the phase transformation accompanying orderly shear deformation without atomic diffusion. The structures made by martensitic transformation are classified as thin plate, lens or lath in steels. The mechanism by which the hierarchic microstructure in the lath martensite phase forms has heretofore not been understood. We have made clear the mechanism by considering, independently, two plastic deformations using the slip deformation model proposed by Khachaturyan, and present herein a deformation matrix for each of the six crystallographic variants in a packet of the hierarchic structure. Our results are quantitatively consistent with experimental results for the K-S crystal-orientation relationship and habit plane. Furthermore, the important points of our study are as follows: (1) the origin of the sub-block structure and the specific combination of the sub-block structure are clarified; (2) the laths existing in a block can be explained; and (3) deviations between the directional parallel and plane parallel are obtained quantitatively, without any adjustable parameters.

Keywords: martensite, lath, structure, plastic, slip, deformation, K-S, orientation relationship, habit plane

1. Introduction

Martensitic transformation is the adiabatic-phase transformation accompanying a change in crystal structure. The martensite phase inevitably contains dislocations or twins as lattice defects that release strain between the martensite crystal and the surrounding untransformed crystal. Minimization of this strain energy determines the morphology of the martensite phase.

There are several kinds of martensite morphologies in steels. Thin-plate martensite contains only internal twins; lens martensite contains both internal twins and dislocations; and lath martensite contains only dislocations. This lath martensite is observed only in steels (ferrous alloys) and is not observed in nonferrous systems. In this study, we focus on lath martensite, whose formation mechanism is not yet understood.

It is reported that the lath martensite phase forms in steels having relatively high martensite start (Ms) temperatures and that the habit plane is near $\{557\}_\gamma$ different by about 10 degrees from $\{111\}_\gamma$ [1] [2]. Its crystal-orientation relationship is nearly K-S, composed of the relationships

$$(111)_\gamma // (011)_{\alpha'}, [\bar{1}01]_\gamma // [\bar{1}\,\bar{1}\,1]_{\alpha'} \quad ,$$

where $(111)_\gamma$ and $(011)_{\alpha'}$ are close-packed planes and $[\bar{1}01]_\gamma$ and $[\bar{1}\,\bar{1}\,1]_{\alpha'}$ are close-packed directions in the austenite phase (γ) and the martensite phase (α′), respectively. A total of 24 crystallographic variants satisfy this orientation relationship as shown in Table 1.

The lath martensite phase possesses a hierarchic structure as shown schematically in Fig. 1. This hierarchy is as follows: (i) A prior austenite grain is composed of *packets*; (ii) A packet is composed of an ensemble of grains, called blocks, which have the same $\{111\}_\gamma$ plane as does the habit plane; and (iii) A block is composed of an ensemble of single martensite crystals called laths, which have nearly the same crystal orientation and high dislocation densities [3] [4].

Crystal orientation in the lath martensite phase was recently analyzed over a relatively wide area using the electron back-scattering pattern (EBSP) measured with a scanning electron microscope (SEM). Before EBSP became available, a block was considered to be composed of an assembly of laths with the same variant (Fig. 2 (a)), separated into regions with small crystallographic inclinations to one another; the inclination boundary was also the lath boundary (broken lines in the figure). However, using EBSP, Morito et al. found that crystal orientation in low-carbon steels deviates locally at each point in a block, and that blocks are composed of not just one but rather a combination of two specific crystallographic variants [2] [3] as illustrated in Fig. 2 (b). For example, grains belonging to variant 4 are observed only in blocks that are composed predominantly of variant 1; similarly, grains belonging to variant 5 are observed only in blocks that are composed predominantly of variant 2 and so on. The boundary between V1 and V4 in the figure, drawn as a solid line, is the block boundary. The researchers called this morphology *sub-blocks* and distinguished it from conventional blocks [2] [3].

Many theories regarding the deformation geometry of martensitic transformation, such as Bowles–MacKenzie (BM) theory and Wechsler–Lieberman–Read (WLR) theory, have been proposed [5][6]. They are collectively called the *phenomenological theory of martensite crystallography* (PTMC). PTMC is based on the experimental observation that deformation with martensitic transformation is invariant plane deformation, because the martensite phase maintains continuity with the surrounding austenite phase. As a result, the martensite phase has the invariant plane as the habit plane. In PTMC, all deformations induced by martensitic transformation are explained by a combination of lattice deformation (as crystal structure changes), lattice-invariant deformation occurring from shear deformations and rigid-body rotation. Well-known examples applying PTMC to lath martensite include studies by Sandvik and Wayman, and Kelly [7][8].

However, it is unlikely that transformation actually occurs in this sequence. In other words, PTMC describes the result of transformation well but does not explain the mechanism of transformation.

Khachaturyan has presented a model describing deformation with martensitic transformation [9]. His model considers all deformations to be a combination of lattice deformation (as crystal structure changes from fcc to bct) and lattice-invariant deformations with plastic deformations by slip. This model is reasonable in its explanation of the transformation mechanism, but has not yet been verified by detailed, quantitative analyses. Also, as far as we know, there is no report of the plastic deformation that considers several slip systems independently. Furthermore, it remains unclear why the lath martensite phase should contain sub-blocks as reported by Morito et al., although the lath martensitic structure is important for its contribution to the strength of steel. Thus, it is important for both practical and academic reasons to clarify the mechanism by which the structure forms.

In this paper, we extend Khachaturyan's slip deformation model by considering two plastic deformations independently without any adjustable parameters. We discuss in detail each crystallographic variant involved in a packet—that is, the six variants V1, V2, V3, V4, V5 and V6 from among a total of 24 variants that satisfy the K-S crystal-orientation relationship (Table 1). Through these discussions, we clarify the formation mechanism of the hierarchic structure in lath martensite in steels. By considering two slip systems independently, it is found for the first time in this paper that the existence of sub-blocks and laths in martensite is clarified as an inevitable consequence of the plastic deformation by slip in martensite transformation.

2. Calculation procedure

In the slip model proposed by Khachaturyan [9], crystal deformations induced by martensitic transformation are described as a combination of lattice deformation from fcc to bct and plastic deformations to release the strain energy caused by lattice deformation.

2.1. Lattice deformation

First, we consider lattice deformation as described by the Bain deformation model [10]. In this model, a tetragonal unit cell exists between two fcc unit cell (Fig. 3 (a)). The bct martensite lattice is made from this tetragonal unit cell by Bain deformation (Figs. 3 (b) and (c)). Here, a_γ is a lattice parameter of the fcc austenite phase, and $a_{\alpha'}$ and $c_{\alpha'}$ are lattice parameters of the bct martensite phase. The length of the a-axis in the tetragonal unit cell before deformation is $a_\gamma / \sqrt{2}$, and the length of the c-axis is a_γ; similarly, the length of the a-axis in the bct unit cell after deformation is $a_{\alpha'}$ and the length of the c-axis is $c_{\alpha'}$. Therefore, these deformations can be expressed by the Bain deformation matrix $\mathbf{B_3}$ as follows:

$$\mathbf{B_3} = \begin{pmatrix} \eta_1 & 0 & 0 \\ 0 & \eta_1 & 0 \\ 0 & 0 & \eta_3 \end{pmatrix}, \tag{1}$$

$$\eta_1 = \sqrt{2} a_{\alpha'} / a_\gamma ,$$

$$\eta_3 = c_{\alpha'} / a_\gamma .$$

The direction relationship [11] between the coordinate systems for the fcc parent phase (austenite phase) and the bct martensite phase is given by

$$\begin{bmatrix} a \\ b \\ c \end{bmatrix}_{\gamma} = \begin{pmatrix} 1/2 & 1/2 & 0 \\ -1/2 & 1/2 & 0 \\ 0 & 0 & 1 \end{pmatrix} \begin{bmatrix} u \\ v \\ w \end{bmatrix}_{\alpha'}. \tag{2}$$

The plane relationship [11] between the two coordinate systems is given by

$$(hkl)_{\gamma} = (pqr)_{\alpha'} \begin{pmatrix} 1 & -1 & 0 \\ 1 & 1 & 0 \\ 0 & 0 & 1 \end{pmatrix}. \tag{3}$$

These relationships are called the *lattice correspondence*. There are six crystallographic variants in a packet (Table 1). When a bct martensite lattice is formed by Bain deformation (Figs. 3 (b) and (c)), we consider which variants are closely related with respect to crystal orientation. The result is the two variants V1 and V4 [3].

The relationship described in Eqs. (1), (2) and (3), and in Figs. 3 (b) and (c), is the case in which the $[001]_{\gamma}$ axis coincides with the $[001]_{\alpha'}$ axis. The $[001]_{\gamma}$, $[100]_{\gamma}$ and $[010]_{\gamma}$ axes are equivalent in fcc austenite crystals, and hence the other two cases in which $[100]_{\gamma}$ coincides with $[001]_{\alpha'}$ and $[010]_{\gamma}$ coincides with $[001]_{\alpha'}$ should also be considered. As shown in Table 1, for the former of the two additional cases, V2 and V5 show the closest crystallographic relationship; for the latter, V3 and V6 show the closest relationship. The three sets of lattice deformations—V1 and V4, V2 and V5, and V3 and V6—are shown in Figs. 4 (a), (b) and (c), respectively.

For the case in which $[100]_\gamma$ coincides with $[001]_{\alpha'}$—that is, for the set of V2 and V5 (Fig. 4 (b))—the Bain deformation matrix $\mathbf{B_1}$ and the lattice correspondence are given by

$$\mathbf{B_1} = \begin{pmatrix} \eta_3 & 0 & 0 \\ 0 & \eta_1 & 0 \\ 0 & 0 & \eta_1 \end{pmatrix}, \tag{4}$$

$$\begin{bmatrix} a \\ b \\ c \end{bmatrix}_\gamma = \begin{pmatrix} 0 & 0 & 1 \\ 1/2 & 1/2 & 0 \\ -1/2 & 1/2 & 0 \end{pmatrix} \begin{bmatrix} u \\ v \\ w \end{bmatrix}_{\alpha'}, \tag{5}$$

$$(hkl)_\gamma = (pqr)_{\alpha'} \begin{pmatrix} 0 & 1 & -1 \\ 0 & 1 & 1 \\ 1 & 0 & 0 \end{pmatrix}. \tag{6}$$

For the case in which $[010]_\gamma$ coincides with $[001]_{\alpha'}$—that is, for the set of V3 and V6 (Fig. 4 (c))—the Bain deformation matrix $\mathbf{B_2}$ and the lattice correspondence are given by

$$\mathbf{B_2} = \begin{pmatrix} \eta_1 & 0 & 0 \\ 0 & \eta_3 & 0 \\ 0 & 0 & \eta_1 \end{pmatrix}, \tag{7}$$

$$\begin{bmatrix} a \\ b \\ c \end{bmatrix}_\gamma = \begin{pmatrix} -1/2 & 1/2 & 0 \\ 0 & 0 & 1 \\ 1/2 & 1/2 & 0 \end{pmatrix} \begin{bmatrix} u \\ v \\ w \end{bmatrix}_{\alpha'}, \tag{8}$$

$$(hkl)_{\gamma} = (pqr)_{\alpha'} \begin{pmatrix} -1 & 0 & 1 \\ 1 & 0 & 1 \\ 0 & 1 & 0 \end{pmatrix}. \tag{9}$$

2.2. Plastic deformations

Lattice deformation is inevitable in martensitic transformation. But its magnitude is so large that a bct martensite crystal cannot exist in the host austenite crystal with only the elastically constrained condition. Therefore, as mentioned previously, plastic deformations of the martensite crystal are needed.

We consider now the case in which the $[001]_{\gamma}$ axis coincides with the $[001]_{\alpha'}$ axis. The elastically constrained condition can be released by plastic deformations along the c-axis in the bct martensite lattice (Fig. 3 (c)). In the simplest case, this relaxation can be accomplished by two slip systems, $[101](\bar{1}01)_{\alpha'}$ and $[\bar{1}01](101)_{\alpha'}$, as shown in Fig. 5 (a). Strictly speaking, neither $[101](\bar{1}01)_{\alpha'}$ nor $[\bar{1}01](101)_{\alpha'}$ are slip systems in bct crystals, but these slips can be made by a combination of two $\mathbf{a}/2\langle 111\rangle_{\alpha'}$ dislocations having the Burgers vectors $\mathbf{b_1}$ and $\mathbf{b_2}$ (Fig. 5 (b)). In fact, it is reported that $\mathbf{a}/2\langle 111\rangle_{\alpha'}$ dislocations reportedly exist in high-density in lath martensite [12].

When bct martensite crystal vector $\mathbf{r}_{\alpha'}$ is transformed into $\mathbf{r'}_{\alpha'}$ by deformation, the relationship between the two vectors is given by

$$\mathbf{r'}_{\alpha'} = \mathbf{r}_{\alpha'} + \mathbf{T}(\mathbf{r}_{\alpha'}), \tag{10}$$

where $\mathbf{T}(\mathbf{r}_{\alpha'})$ is total displacement. Because total displacement is generated by deformations in

the $[101]_{\alpha'}$ and $[\bar{1}01]_{\alpha'}$ directions, $\mathbf{T}(\mathbf{r}_{\alpha'})$ can be written as

$$\mathbf{T}(\mathbf{r}_{\alpha'}) = \mathbf{T}_{[101]_{\alpha'}} n_1 + \mathbf{T}_{[\bar{1}01]_{\alpha'}} n_2 , \tag{11}$$

where n_1 and n_2 are the numbers of active slip planes, and $\mathbf{T}_{[101]_{\alpha'}}$ and $\mathbf{T}_{[\bar{1}01]_{\alpha'}}$ are the displacements in each slip direction. In addition, n_1 and n_2 can be written as

$$n_1 = \frac{1}{m_1} \mathbf{H}_{(\bar{1}01)_{\alpha'}} \mathbf{r}_{\alpha'} , \tag{12}$$

$$n_2 = \frac{1}{m_2} \mathbf{H}_{(101)_{\alpha'}} \mathbf{r}_{\alpha'} , \tag{13}$$

where m_1 and m_2 are the average numbers of lattice planes between the nearest active slip plane in each slip system, $\mathbf{H}$ is a reciprocal lattice vector and $\mathbf{H}_{(hkl)_{\alpha'}} \mathbf{r}_{\alpha'}$ is the total number of $(hkl)_{\alpha'}$ planes within the length of the vector $\mathbf{r}_{\alpha'}$. Substituting Eqs. (11), (12) and (13) into Eq. (10), we get

$$\mathbf{r'}_{\alpha'} = \left(\mathbf{I} + \frac{1}{m_1} \mathbf{T}_{[101]_{\alpha'}} * \mathbf{H}_{(\bar{1}01)_{\alpha'}} + \frac{1}{m_2} \mathbf{T}_{[\bar{1}01]_{\alpha'}} * \mathbf{H}_{(101)_{\alpha'}} \right) \mathbf{r}_{\alpha'} . \tag{14}$$

where $\mathbf{I}$ is the unit matrix. In Eq. (14),

$$\left(\mathbf{I} + \frac{1}{m_1} \mathbf{T}_{[101]_{\alpha'}} * \mathbf{H}_{(\bar{1}01)_{\alpha'}} + \frac{1}{m_2} \mathbf{T}_{[\bar{1}01]_{\alpha'}} * \mathbf{H}_{(101)_{\alpha'}} \right) \tag{15}$$

is a matrix that transforms vector $\mathbf{r}_{\alpha'}$ into $\mathbf{r'}_{\alpha'}$. In other words, Eq. (15) is a matrix representing the plastic deformations.

2.3. Total deformation in the martensite phase

The procedure mentioned in sections 2.1. and 2.2. describes lattice deformation according to the Bain deformation and plastic deformations for releasing strain caused by lattice deformation. The total deformation that occurs by martensitic transformation can thus be evaluated by this procedure.

From Eq. (1), transformation of vector $\mathbf{r}_{\gamma}$ (austenite phase) into $\mathbf{r}_{\alpha'}$ by lattice deformation is written as

$$\mathbf{r}_{\alpha'} = \mathbf{B_3}\mathbf{r}_{\gamma}. \tag{16}$$

Substituting Eq. (16) into Eq. (14), we get

$$\mathbf{r'}_{\alpha'} = \left(\mathbf{IB_3} + \frac{1}{m_1}\mathbf{T}_{[101]_{\alpha'}} * \mathbf{H}_{(\bar{1}01)_{\alpha'}}\mathbf{B_3} + \frac{1}{m_2}\mathbf{T}_{[\bar{1}01]_{\alpha'}} * \mathbf{H}_{(101)_{\alpha'}}\mathbf{B_3} \right)\mathbf{r}_{\gamma}. \tag{17}$$

Using Eq. (2), we can express the total displacement along $[101]_{\alpha'}$ using the total displacements along $\left[\frac{1}{2}\frac{\bar{1}}{2}1\right]_{\gamma}$ and that along $[\bar{1}01]_{\alpha'}$ using the total displacements along $\left[\frac{\bar{1}}{2}\frac{1}{2}1\right]_{\gamma}$. Thus, we obtain the equations

$$\mathbf{T}_{[\mathbf{101}]_{\alpha'}} = \mathbf{B_3}\mathbf{T}_{\left[\frac{\mathbf{1}}{\mathbf{2}}\frac{\bar{\mathbf{1}}}{\mathbf{2}}\mathbf{1}\right]_{\gamma}} = \begin{pmatrix} \eta_1 & 0 & 0 \\ 0 & \eta_1 & 0 \\ 0 & 0 & \eta_3 \end{pmatrix} \begin{pmatrix} \frac{a_\gamma}{2} \\ -\frac{a_\gamma}{2} \\ a_\gamma \end{pmatrix} = \begin{pmatrix} \frac{a_\gamma}{2}\eta_1 \\ -\frac{a_\gamma}{2}\eta_1 \\ a_\gamma\eta_3 \end{pmatrix}, \tag{18}$$

$$\mathbf{T}_{[\bar{\mathbf{1}}\mathbf{01}]_{\alpha'}} = \mathbf{B_3}\mathbf{T}_{\left[\frac{\bar{\mathbf{1}}}{\mathbf{2}}\frac{\mathbf{1}}{\mathbf{2}}\mathbf{1}\right]_{\gamma}} = \begin{pmatrix} \eta_1 & 0 & 0 \\ 0 & \eta_1 & 0 \\ 0 & 0 & \eta_3 \end{pmatrix} \begin{pmatrix} -\frac{a_\gamma}{2} \\ \frac{a_\gamma}{2} \\ a_\gamma \end{pmatrix} = \begin{pmatrix} -\frac{a_\gamma}{2}\eta_1 \\ \frac{a_\gamma}{2}\eta_1 \\ a_\gamma\eta_3 \end{pmatrix}, \tag{19}$$

From the relationship

$$\mathbf{H}_{(\mathbf{pqr})_{\alpha'}} = \mathbf{H}_{(\mathbf{hkl})_{\gamma}}\mathbf{B}_{\mathbf{3}}^{-\mathbf{1}}, \tag{20}$$

we get the equation

$$\mathbf{H}_{(\mathbf{pqr})_{\alpha'}}\mathbf{B_3} = \mathbf{H}_{(\mathbf{hkl})_{\gamma}}. \tag{21}$$

Using Eqs. (3) and (21), $\mathbf{H}_{(\bar{\mathbf{1}}\mathbf{01})_{\alpha'}}\mathbf{B_3}$ in Eq. (17) can be written as $\mathbf{H}_{(\bar{\mathbf{1}}\mathbf{11})_{\gamma}}$ and $\mathbf{H}_{(\mathbf{101})_{\alpha'}}\mathbf{B_3}$ in Eq. (17) can be written as $\mathbf{H}_{(\mathbf{1}\bar{\mathbf{1}}\mathbf{1})_{\gamma}}$. Thus, we obtain the equations

$$\mathbf{H}_{(\bar{1}01)_{\alpha'}}\mathbf{B}_3 = \mathbf{H}_{(\bar{1}11)_{\gamma}} = \begin{pmatrix} -\dfrac{1}{a_\gamma} \\ \dfrac{1}{a_\gamma} \\ \dfrac{1}{a_\gamma} \end{pmatrix}, \tag{22}$$

$$\mathbf{H}_{(101)_{\alpha'}}\mathbf{B}_3 = \mathbf{H}_{(1\bar{1}1)_{\gamma}} = \begin{pmatrix} \dfrac{1}{a_\gamma} \\ -\dfrac{1}{a_\gamma} \\ \dfrac{1}{a_\gamma} \end{pmatrix}. \tag{23}$$

Substituting Eqs. (18), (19), (22) and (23) into Eq. (17), we get

$$\mathbf{r'}_{\alpha'} = \begin{pmatrix} \left(1-\dfrac{1}{2m_1}-\dfrac{1}{2m_2}\right)\eta_1 & \left(\dfrac{1}{2m_1}+\dfrac{1}{2m_2}\right)\eta_1 & \left(\dfrac{1}{2m_1}-\dfrac{1}{2m_2}\right)\eta_1 \\ \left(\dfrac{1}{2m_1}+\dfrac{1}{2m_2}\right)\eta_1 & \left(1-\dfrac{1}{2m_1}-\dfrac{1}{2m_2}\right)\eta_1 & \left(-\dfrac{1}{2m_1}+\dfrac{1}{2m_2}\right)\eta_1 \\ \left(-\dfrac{1}{m_1}+\dfrac{1}{m_2}\right)\eta_3 & \left(\dfrac{1}{m_1}-\dfrac{1}{m_2}\right)\eta_3 & \left(1+\dfrac{1}{m_1}+\dfrac{1}{m_2}\right)\eta_3 \end{pmatrix} \mathbf{r}_\gamma . \tag{24}$$

Finally,

$$\begin{pmatrix} \left(1-\dfrac{1}{2m_1}-\dfrac{1}{2m_2}\right)\eta_1 & \left(\dfrac{1}{2m_1}+\dfrac{1}{2m_2}\right)\eta_1 & \left(\dfrac{1}{2m_1}-\dfrac{1}{2m_2}\right)\eta_1 \\ \left(\dfrac{1}{2m_1}+\dfrac{1}{2m_2}\right)\eta_1 & \left(1-\dfrac{1}{2m_1}-\dfrac{1}{2m_2}\right)\eta_1 & \left(-\dfrac{1}{2m_1}+\dfrac{1}{2m_2}\right)\eta_1 \\ \left(-\dfrac{1}{m_1}+\dfrac{1}{m_2}\right)\eta_3 & \left(\dfrac{1}{m_1}-\dfrac{1}{m_2}\right)\eta_3 & \left(1+\dfrac{1}{m_1}+\dfrac{1}{m_2}\right)\eta_3 \end{pmatrix} \tag{25}$$

is the matrix that represents the total deformation caused by both lattice deformation and plastic deformations. V1 or V4 can be determined using the deformation expressed by this matrix.

2.4. Determination of the quantitative value of the total deformation

To prove the validity of Eq. (25) in describing deformation by martensitic transformation, we consider deviations between the calculated invariant plane and the habit plane observed in lath martensite steels. We also examine deviations from the K-S crystal-orientation relationship with respect to close-packed planes and close-packed directions.

Eigenvalues of the matrix in Eq. (25), in ascending order, are λ_1, λ_2 and λ_3; the corresponding eigenvectors are $\mathbf{e_1}$, $\mathbf{e_2}$ and $\mathbf{e_3}$. The condition that the matrix gives an invariant plane deformation is $\lambda_1 < 1, \lambda_2 = 1, \lambda_3 > 1$, [14] (see Appendix). When this condition is satisfied, the normal vector $\mathbf{n}$ of the invariant plane is given by

$$\mathbf{n} = \sqrt{\frac{1-\lambda_1^2}{\lambda_3^2-\lambda_1^2}}\mathbf{e_1} + \sqrt{\frac{\lambda_3^2-1}{\lambda_3^2-\lambda_1^2}}\mathbf{e_3} \quad . \tag{26}$$

Let the vector in the direction of strain be $\mathbf{l}$ and the amount of strain be ε_0. We then have

$$\mathbf{l} = -\lambda_3\sqrt{\frac{1-\lambda_1^2}{\lambda_3^2-\lambda_1^2}}\mathbf{e_1} + \lambda_1\sqrt{\frac{\lambda_3^2-1}{\lambda_3^2-\lambda_1^2}}\mathbf{e_3}\,, \tag{27}$$

$$\varepsilon_0 = \lambda_3 - \lambda_1\,. \tag{28}$$

Then normal vector $\mathbf{H}_{(pqr)_{\alpha'}}$ of an arbitrary plane in the reciprocal space and the vector $\mathbf{T}_{[uvw]_{\alpha'}}$ of

an arbitrary direction in the martensite lattice are given by

$$\mathbf{H}_{(pqr)_{\alpha'}} = \mathbf{H}_{(hkl)_{\gamma}} - \frac{\varepsilon_0 \left(\mathbf{l}\mathbf{H}_{(hkl)_{\gamma}}\right)}{\left\{1 + \varepsilon_0 (\mathbf{ln})\right\}}\mathbf{n}\,, \tag{29}$$

$$\mathbf{T}_{[uvw]_{\alpha'}} = \mathbf{T}_{[abc]_{\gamma}} + \varepsilon_0 \mathbf{l}\left(\mathbf{n}\mathbf{T}_{[abc]_{\gamma}}\right). \tag{30}$$

The relationship between the $(pqr)_{\alpha'}$ and $(hkl)_{\gamma}$ planes satisfies the lattice correspondence in Eq. (3), and the relationship between the $[uvw]_{\alpha'}$ and $[abc]_{\gamma}$ directions satisfies the lattice correspondence in Eq. (2).

To investigate the reliability of the deformation in Eq. (25), we evaluated the angular deviation between the normal vector of the invariant plane in Eq. (26) and the normal vector of the $\{557\}_{\gamma}$ habit plane reported by experimental observations by calculating the scalar products between the two vectors.

To determine the crystal-orientation relationship, first we calculated the normal vector of $(011)_{\alpha'}$ with Eq. (29) and evaluated angular deviations between the normal vectors $(111)_{\gamma}$ and $(011)_{\alpha'}$. Then we calculated each vector of $\langle 111 \rangle_{\alpha'}$, which are the close-packed directions of V1 and V4 listed in Table 1, with Eq. (30), and evaluated angular deviations between the vectors $\left[\bar{1}01\right]_{\gamma}$ and $\left[\bar{1}\,\bar{1}1\right]_{\alpha'}$ as well as between $\left[01\bar{1}\right]_{\gamma}$ and $\left[\bar{1}1\,\bar{1}\right]_{\alpha'}$. Although m_1 and m_2 should be integer in a crystal, all calculations were conducted as real for m_1 and m_2 in order to obtain the rigorous invariant plane deformation condition, that is, $\lambda_2 = 1$.

3. Calculated results

3.1. Deformation matrix

As mentioned in Section 2.3, the deformation matrix for the lattice deformation corresponding to V1 and V4 (Fig. 4 (a)) is given by Eq. (25). Similarly, the matrix for V2 and V5 (Fig. 4 (b)) is given by

$$\begin{pmatrix} \left(1+\frac{1}{m_1}+\frac{1}{m_2}\right)\eta_3 & \left(-\frac{1}{m_1}+\frac{1}{m_2}\right)\eta_3 & \left(\frac{1}{m_1}-\frac{1}{m_2}\right)\eta_3 \\ \left(\frac{1}{2m_1}-\frac{1}{2m_2}\right)\eta_1 & \left(1-\frac{1}{2m_1}-\frac{1}{2m_2}\right)\eta_1 & \left(\frac{1}{2m_1}+\frac{1}{2m_2}\right)\eta_1 \\ \left(-\frac{1}{2m_1}+\frac{1}{2m_2}\right)\eta_1 & \left(\frac{1}{2m_1}+\frac{1}{2m_2}\right)\eta_1 & \left(1-\frac{1}{2m_1}-\frac{1}{2m_2}\right)\eta_1 \end{pmatrix} \tag{31}$$

and the matrix for V3 and V6 is given by

$$\begin{pmatrix} \left(1-\frac{1}{2m_1}-\frac{1}{2m_2}\right)\eta_1 & \left(-\frac{1}{2m_1}+\frac{1}{2m_2}\right)\eta_1 & \left(\frac{1}{2m_1}+\frac{1}{2m_2}\right)\eta_1 \\ \left(\frac{1}{m_1}-\frac{1}{m_2}\right)\eta_3 & \left(1+\frac{1}{m_1}+\frac{1}{m_2}\right)\eta_3 & \left(-\frac{1}{m_1}+\frac{1}{m_2}\right)\eta_3 \\ \left(\frac{1}{2m_1}+\frac{1}{2m_2}\right)\eta_1 & \left(\frac{1}{2m_1}-\frac{1}{2m_2}\right)\eta_1 & \left(1-\frac{1}{2m_1}-\frac{1}{2m_2}\right)\eta_1 \end{pmatrix}. \tag{32}$$

Using these matrices, each invariant plane vector $\mathbf{n}$, normal vector $\mathbf{H}_{(pqr)_{\alpha'}}$ of an arbitrary plane and vector $\mathbf{T}_{[uvw]\alpha'}$ of an arbitrary direction are obtained when the eigenvalue in each matrix satisfies the condition $\lambda_2 = 1$, as mentioned in Section 2.4. In Eq. (32), m_1 and m_2 are variables. For 0.1% C steel, the lattice parameters used in these calculations are

$a_\gamma = 3.599 \times 10^{-10} m$, $a_{\alpha'} = 2.8667 \times 10^{-10} m$, and $c_{\alpha'} = 2.8796 \times 10^{-10} m$, according to the empirical formula $(c/a)_{\alpha'} = 1 + 0.045[\%C]$.

3.2. Angular deviation between the calculated invariant plane and the observed habit plane

Figure 6 (a) shows the relationship between m_1 and m_2 when the eigenvalue of $\lambda_2 = 1$ is satisfied for V1 and V4. Figure 6 (b) shows the plot of the angular deviation between the calculated invariant plane (the normal vector **n**) and the observed habit plane $(557)_\gamma$ against the m_1 value, and the arrows correspond to those in Fig. 6 (a). In Figs. 6 (a) and (b), m_1 and m_2 are not independent of each other under the condition $\lambda_2 = 1$. In other words, the independent variables m_1 and m_2 are determined unambiguously as an inevitable result of the invariant plane deformation condition of $\lambda_2 = 1$. When $m_1 = m_2 = 17.8$, the angular deviation between the calculated invariant plane and the normal vector of the observed habit plane reaches the minimum value of 3.36 degree, as indicated by the open circles in Figs. 6 (a) and (b). According to lattice equivalence (Fig. 4), the habit planes are as follows: for V1 and V4, $(557)_\gamma$ (Fig. 4 (a)); for V2 and V5, $(755)_\gamma$ (Fig. 4 (b)); and for V3 and V6, $(575)_\gamma$ (Fig. 4 (c)). The relationship between the m_i $(i = 1, 2)$ values and the angular deviation, as shown in Figs. 6 (a) and (b), is the same for each equivalent lattice.

3.3. Angular deviation from the K–S orientation relationship

Figure 7 shows the angular deviations between $(111)_\gamma$ and $(011)_{\alpha'}$, between the equivalent close-packed directions $\left[\bar{1}01\right]_\gamma$ and $\left[\bar{1}\bar{1}1\right]_{\alpha'}$ (for V1), and between the equivalent close-packed directions $\left[01\bar{1}\right]_\gamma$ and $\left[\bar{1}1\bar{1}\right]_{\alpha'}$ (for V4), calculated from the deformation matrix Eq.

(25) for V1 and V4. The $(111)_\gamma$ and $(011)_{\alpha'}$ planes are close packed in each lattice system, and they should be parallel in a K–S orientation relationship. In addition, each set of two close-packed directions should be parallel according to the K–S orientation relationship.

The angular deviation between $(111)_\gamma$ and $(011)_{\alpha'}$ reaches the minimum value of approximately 0.17 degree at $m_1 = 17.8$, indicated by the open circle in Fig. 7. The position of this open circle is exactly consistent with the angular deviation in Fig. 6 (a) ($m_1 = m_2 = 17.8$). In contrast, the angular deviation between the equivalent close-packed directions exhibits the minimum value of zero at $m_1 = 28.6$ for V1, indicated by the open triangle, and at $m_1 = 14.4$ for V4, indicated by the open square in Fig. 7. In these two cases, $m_2 = 14.4$ for V1 and $m_2 = 28.6$ for V4, because m_1 and m_2 are not independent of each other, as mentioned in Section 3.2. The corresponding open square and triangle are also plotted in Fig. 6 (a). These results show that the K–S relationship in the close-packed direction is well satisfied when deformation is greater in one direction than in the other.

The calculation results of angular deviations are summarized in Table 2. In the table, only one variant set originates from the same lattice deformation, that is, V1 and V4, but the other variant sets for V2 and V5 and for V3 and V6 can be obtained using the same symmetry relationships with respect to m_1 and m_2. Hence, the results show that the two close-packed planes are almost parallel (see the column "Plane parallel" in Table 2). The K–S orientation relationship is thus satisfied for a relatively wide range of m_i ($i = 1, 2$) values. That is, both m_1 and m_2 are approximately greater than 14 (see also Fig. 7), although they do not change independently of each other; rather, they change along the line in Fig. 6 (a). The angular deviation between the close-packed planes reaches a minimum at $m_1 = m_2 = 17.8$.

4. Discussion

As shown in Fig. 6 and Table 2, the angular deviation between the invariant plane and the observed habit plane reaches a minimum at $m_1 = m_2 = 17.8$. To discuss the variant relationships, we consider the angular deviation for the calculated invariant planes from the $\{557\}_\gamma$ habit plane obtained experimentally (Fig. 6 (b)), close-packed planes in the K–S orientation relationship, and close-packed directions in the K–S orientation relationship with m_1 (Fig. 7). The angular deviations between each calculated invariant plane and the $\{557\}_\gamma$ habit plane reach a minimum when $m_1 = m_2 = 17.8$ (Table 2), as indicated by the open circles in Figs. 6 (a) and (b). In this condition, the angular deviations from the close-packed direction, which are denoted by solid and broken lines in Fig. 7, become equal (0.64 degree in Table 2), as indicated by the arrow in Fig. 7. That is, the angular deviation from the close-packed direction for V1 is equal to that for V4 (Table 2). This fact indicates that there is an equal possibility of V1 and V4 in martensite crystal. The same situation occurs for V2 and V5 as well as for V3 and V6. Consequently, if $m_1 = m_2 = m$, it is impossible to distinguish these two sets of variants in the K–S orientation relationship. If $m_1 > m_2$, deviation becomes small for V1; in other words, V1 is formed by slip deformation (Table 2). Similarly, if $m_2 > m_1$, V4 becomes stable (Table 2). In the same manner, V3 and V5 become stable if $m_1 > m_2$ and V2 and V6 are stable if $m_2 > m_1$. These results are obtained by calculating Eqs. (31) and (32).

Thus, it can be inferred that each variant of lath martensite is determined by the magnitude of m_1 and m_2. This indicates that formation of the variant is determined by a combination of lattice deformation and two kinds of subsequent plastic deformations. In particular, V1 forms by lattice deformation as per Eq. (25) and subsequent plastic deformations primarily consisting of the $[\bar{1}01](101)_{\alpha'}$ system, which can be produced by $\mathbf{a}/2[\bar{1}11]$ and $\mathbf{a}/2[\bar{1}\bar{1}1]$ on $(101)_{\alpha'}$ slip

systems. Similarly, V2 is characterized by Eq. (31) and the $[101](\bar{1}01)_{\alpha'}$ system, V3 by Eq. (32) and the $[\bar{1}01](101)_{\alpha'}$ system, V4 by Eq. (25) and the $[101](\bar{1}01)_{\alpha'}$ system, V5 by Eq. (31) and the $[\bar{1}01](101)_{\alpha'}$ system, and V6 by Eq. (32) and the $[101](\bar{1}01)_{\alpha'}$ system.

The rule of variant determination mentioned above is not related m_i $(i=1,2)$. In other words, it is not necessary for a variant to have a unique m_i value. This indicates that a particular variant is not always formed by the same specific magnitude of plastic deformation, and the magnitudes vary widely. Each single lath crystal is a region with a unique m_i value, and a block is a region with multiple m_i values, that is, an aggregation of single laths with slightly different m_i values. This is consistent with the experimental observation that a block is an aggregation of laths that are slightly misoriented with respect to each other (Fig. 8 (a)) [3]. The sub-blocks reported by Morito et al. are invariably observed as a peculiar combination of variants originating from the same lattice deformations: V1 and V4, V2 and V5, and V3 and V6. These are regions of alternating magnitudes of m_1 and m_2 (Fig. 8 (b)). Inevitability of the existence of sub-blocks and laths in a block is clarified by the present study employing for the first time two kinds of plastic deformations in martensitic transformation of steels. In other words, two kinds of slip systems need substantially to form sub-blocks and laths, and this is absolutely different from Khachaturyan's approach.

Regarding the K–S orientation relationships, as can be seen in Fig. 7 and Table 2, the value of $m_1(m_2)$ for the relationship of close-packed planes is different from that of close-packed directions. Hence, the plane parallel and the direction parallel relationships cannot be simultaneously satisfied. This is the reason that lath martensite steels satisfy the relationship of close-packed planes with high accuracy but deviate from the relationship of close-packed directions, as reported by experimental observations [14].

5. Conclusions

To clarify the formation mechanism of the lath martensite phase in steels, we extended Khachaturyan's deformation model and examined deformations accompanying martensitic transformation by considering two independent plastic deformations for six variants belonging to a packet. We obtained the following conclusions:

1. The experimental observations showed that lath martensite has six crystallographic variants, an invariant plane, and the K–S orientation relationship. These observations can be explained by a combination of lattice deformation by Bain correspondence and subsequent plastic deformations corresponding to the two slip systems $[101](\bar{1}01)_{\alpha'}$ and $[\bar{1}01](101)_{\alpha'}$, both of which can be produced by a combination of two $\mathbf{a}/2\langle 111\rangle_{\alpha'}$.

2. Lattice deformation determines the variants; the magnitude of the two subsequent plastic deformations determines the identity of the variants. The two variants belonging to a sub-block are generated by the same lattice deformation. Only a difference in the magnitude of the two subsequent plastic deformations causes the variants to differ. Hence, a sub-block always contains the same two variants.

3. A particular variant is not always formed by the same specific magnitude of plastic deformation; rather, the magnitudes of plastic deformation widely vary. A single lath is generated by a specific magnitude of plastic deformation, and a block is generated by a slightly different magnitude of plastic deformation, resulting in small misorientations between laths.

4. The magnitude of plastic deformation that satisfies the parallel relationship of close-packed planes in the K–S orientation relationship is different from that which satisfies the parallel relationship of close-packed directions in the K–S orientation relationship. Hence, both relationships cannot be satisfied simultaneously. This is the reason that lath martensite steels deviate from the K–S relationship with respect to close-packed directions. Thus, the calculations in this paper coincide well with the observed facts.

Acknowledgement

This work was supported partly by the Grant-in-Aid for Scientific Research of Japan Society for the Promotion of Science (JSPS), Japan.

References

[1] A.R. Marder, G. Krauss: A.S.M. Transactions quarterly. 62, 4 (1969), 957-964.

[2] S. Morito: Acta Materiallia. 54 (2006), 5323-5331.

[3] S. Morito: Acta Materialia. 51 (2003), 1789-1799.

[4] H. Kitahara: Acta Materialia. 54 (2006), 1279-1288.

[5] J.S. Bowles, J.K.MacKenzie: Acta Metallurgica. 2 (1954), 129-137, 138-147, 224-234.

[6] M.S. Wechsler, D.S. Lieberman, T.A. Read: Transaction of the American Institute of Mining and Metallurgical Engineers. 197, 11 (1953), 1503-1515.

[7] B.P.J. Sandvik, C.M. Wayman: Metallugical Transactions A. 14A (1983), 835-844.

[8] P.M. Kelly: Materials Transactions. JIM. 33, 3 (1992), 235-242.

[9] A.G. Khachaturyan: Theory of Structural Transformations in Solids. New York. Wiley (1983).

[10] C.M. Wayman: Introduction to the Crystallography of Martensitic Transformations. New York. Macmillan (1964).

[11] M. Kato: Materials Transactions. JIM. 33, 2 (1992), 89-96.

[12] B.P.J. Sandvik, C.M.Wayman: Metallurgical Transactions A. 14A (1983), 809-822.

[13] J.W. Christian: The theory of Transformations in Metals and Alloys. Oxford. Pergamon (1965).

[14] P.M. Kelly: Acta Metallurgica et Materialia. 38 (1990), 1075-1081.

Appendix

The condition of eigenvalues of the deformation matrix for representing invariant plane deformation

We consider the case that vector $\mathbf{x}_\alpha$ is transformed into $\mathbf{y}_\alpha$ in orthonormal coordinate system α. When the matrix that represents this transformation is written as $\mathbf{S}_\alpha$,

$$\mathbf{y}_\alpha = \mathbf{S}_\alpha \mathbf{x}_\alpha . \tag{A-1}$$

In general, a homogeneous deformation can be regarded as a combination of a pure deformation and a rigid rotation. Thus, we can write the deformation matrix $\mathbf{S}_\alpha$ in the form

$$\mathbf{S}_\alpha = \mathbf{R}_\alpha \mathbf{P}_\alpha . \tag{A-2}$$

where $\mathbf{P}_\alpha$ is the pure dilatation matrix (diagonal matrix) and $\mathbf{R}_\alpha$ is the rigid rotation matrix.

With (A-1) and (A-2), we get the expression

$$\mathbf{y}_\alpha = \mathbf{R}_\alpha \mathbf{P}_\alpha \mathbf{x}_\alpha . \tag{A-3}$$

Now we define the matrix that transforms the coordinate system from α to β as $\mathbf{L}$. Transformation of the coordinate system from β to α is thus written as $\mathbf{L}^{-1}$. Transformation of vector $\mathbf{x}_\beta$ (= $\mathbf{x}_\alpha$ in coordinate system α) into $\mathbf{y}_\beta$ (= $\mathbf{y}_\alpha$ in coordinate system α) in coordinate system β is written as

$$\mathbf{y}_\beta = \mathbf{S}_\beta \mathbf{x}_\beta , \tag{A-4}$$

where $\mathbf{S}_\beta$ is the transformation matrix that represents deformation in coordinate system β.

Now, from the following two relationships,

$$\mathbf{x}_\alpha = \mathbf{L}^{-1} \mathbf{x}_\beta , \tag{A-5}$$

$$\mathbf{y}_\alpha = \mathbf{L}^{-1} \mathbf{y}_\beta , \tag{A-6}$$

Eq. (A-1) is written as

$$\mathbf{L}^{-1}\mathbf{y}_\beta = \mathbf{S}_\alpha \mathbf{L}^{-1}\mathbf{x}_\beta . \tag{A-7}$$

Multiplying Eq. (A-7) by $\mathbf{L}$, we get

$$\mathbf{y}_\beta = \mathbf{L}\mathbf{S}_\alpha \mathbf{L}^{-1}\mathbf{x}_\beta . \tag{A-8}$$

Comparing this equation to Eq. (A-4), we get

$$\mathbf{S}_\beta = \mathbf{L}\mathbf{S}_\alpha \mathbf{L}^{-1} . \tag{A-9}$$

Similarly, for pure dilatation $\mathbf{P}$, we get

$$\mathbf{P}_\beta = \mathbf{L}\mathbf{P}_\alpha \mathbf{L}^{-1} , \tag{A-10}$$

$$\mathbf{P}_\alpha = \mathbf{L}^{-1}\mathbf{P}_\beta \mathbf{L} . \tag{A-11}$$

Rewriting Eq. (A-4) using Eqs. (A-2), (A-9) and (A-11) gives us

$$\begin{aligned} \mathbf{y}_\beta &= \mathbf{S}_\beta \mathbf{x}_\beta \\ &= \mathbf{L}\mathbf{S}_\alpha \mathbf{L}^{-1}\mathbf{x}_\beta \\ &= \mathbf{L}\mathbf{R}_\alpha \mathbf{P}_\alpha \mathbf{L}^{-1}\mathbf{x}_\beta \\ &= \mathbf{L}\mathbf{R}_\alpha \mathbf{L}^{-1}\mathbf{P}_\beta \mathbf{L}\mathbf{L}^{-1}\mathbf{x}_\beta \\ &= \mathbf{L}\mathbf{R}_\alpha \mathbf{L}^{-1}\mathbf{P}_\beta \mathbf{x}_\beta \end{aligned} \quad . \tag{A-12}$$

When the deformation is invariant plane deformation, vectors on the invariant plane remain unchanged in length, so the following equation should be satisfied

$$\begin{aligned} \mathbf{y}'_\beta \, \mathbf{y}_\beta &= \mathbf{x}'_\beta \, \mathbf{P}'_\beta \, \mathbf{L}^{-1\prime} \mathbf{R}'_\alpha \, \mathbf{L}' \mathbf{L}\mathbf{R}_\alpha \mathbf{L}^{-1}\mathbf{P}_\beta \mathbf{x}_\beta \\ &= \mathbf{x}'_\beta \, \mathbf{P}'_\beta \, \mathbf{P}_\beta \mathbf{x}_\beta \\ &= \mathbf{x}'_\beta \, \mathbf{x}_\beta \end{aligned} \quad , \tag{A-13}$$

where ‘prime’ denotes the index of matrices representing the transposition.

From Eq. (A-13), the condition enabling invariant plane deformation is

$$\mathbf{x}'_{\beta}\,\mathbf{P}'_{\beta}\,\mathbf{P}_{\beta}\mathbf{x}_{\beta} = \mathbf{x}'_{\beta}\,\mathbf{x}_{\beta}\,. \tag{A-14}$$

Now, we write the eigenvalues of the matrix $\mathbf{S}_{\beta}$ as λ_i. Using the equation

$$\begin{aligned}\mathbf{S}_{\beta}'\mathbf{S}_{\beta} &= \mathbf{P}_{\beta}'\mathbf{R}_{\beta}'\mathbf{R}_{\beta}\mathbf{P}_{\beta}\\ &= \mathbf{P}_{\beta}'\mathbf{P}_{\beta}\\ &= \mathbf{P}_{\beta}^2\end{aligned}\,, \tag{A-15}$$

we find that eigenvalues of the matrix $\mathbf{S}'_{\beta}\,\mathbf{S}_{\beta}$, i.e. λ_i^2, are the square of each eigenvalue of the matrix $\mathbf{P}_{\beta}$, where $\mathbf{P}_{\beta}$ is a diagonal matrix with eigenvalue λ_i and is written as

$$\mathbf{P}_{\beta} = \left(\lambda_i \delta_{ij}\right). \tag{A-16}$$

Using Eq. (A-16), Eq. (A-14) becomes

$$\lambda_i^2 x_{\beta i}^2 = x_{\beta i}^2\,. \tag{A-17}$$

Eq. (A-17) is expressed in the form

$$\left(\lambda_i^2 - 1\right)x_{\beta i}^2 = \left(\lambda_i^2 - 1\right)x_{\beta i}^2 + \left(\lambda_j^2 - 1\right)x_{\beta j}^2 + \left(\lambda_k^2 - 1\right)x_{\beta k}^2 = 0\,. \tag{A-18}$$

For the invariant plane, $x_{\beta j} = 0$, and hence we get

$$\frac{\lambda_i^2 - 1}{\lambda_k^2 - 1} = -\frac{x_{\beta k}^2}{x_{\beta i}^2}\,. \tag{A-19}$$

For a real solution to Eq. (A-19), the sign of $\left(\lambda_i^2 - 1\right)$ must differ from the sign of $\left(\lambda_k^2 - 1\right)$. Therefore, in the matrix representing invariant plane deformation, three eigenvalues of the matrix are less than 1, equal to 1 and greater than 1.

Captions

Table 1 All 24 crystallographic variants that satisfy the K–S orientation relationship

Table 2 Calculation results of angular deviations for V1 and V4

Fig. 1 Lath martensite hierarchic structure

Fig. 2 Block-grain structure

Fig. 3 Lattice deformation

Fig. 4 Three types of lattice deformations that occur in a packet

Fig. 5 Plastic deformations by slips for V1 and V4

Fig. 6 Calculation result of the deformation matrix Eq. (25) when the eigenvalue of $\lambda_2 = 1$. (a) relationship between m_1 and m_2 values, (b) plot of angular deviation between the calculated invariant plane and the observed habit plane $(557)_\gamma$ against the m_1 value.

Fig. 7 Angular deviations between $(111)_\gamma$ and $(011)_{\alpha'}$, between the equivalent close-packed directions $[\bar{1}01]_\gamma$ and $[\bar{1}\bar{1}1]_{\alpha'}$ (for V1), and between the equivalent close-packed directions $[01\bar{1}]_\gamma$ and $[\bar{1}1\bar{1}]_{\alpha'}$ (for V4), calculated from the deformation matrix Eq. (25) for V1 and V4.

Fig. 8 Block region with varying *m* values.

Variant	Plane parallel	Direction parallel	Variant	Plane parallel	Direction parallel
V1	$(111)_\gamma // (011)_{\alpha'}$	$[\bar{1}01]_\gamma // [\bar{1}\,\bar{1}\,1]_{\alpha'}$	V13	$(\bar{1}11)_\gamma // (011)_{\alpha'}$	$[0\bar{1}1]_\gamma // [\bar{1}\,\bar{1}\,1]_{\alpha'}$
V2		$[\bar{1}01]_\gamma // [\bar{1}1\bar{1}]_{\alpha'}$	V14		$[0\bar{1}1]_\gamma // [\bar{1}1\bar{1}]_{\alpha'}$
V3		$[01\bar{1}]_\gamma // [\bar{1}\,\bar{1}\,1]_{\alpha'}$	V15		$[\bar{1}0\bar{1}]_\gamma // [\bar{1}\,\bar{1}\,1]_{\alpha'}$
V4		$[01\bar{1}]_\gamma // [\bar{1}1\bar{1}]_{\alpha'}$	V16		$[\bar{1}0\bar{1}]_\gamma // [\bar{1}1\bar{1}]_{\alpha'}$
V5		$[1\bar{1}0]_\gamma // [\bar{1}\,\bar{1}\,1]_{\alpha'}$	V17		$[110]_\gamma // [\bar{1}\,\bar{1}\,1]_{\alpha'}$
V6		$[1\bar{1}0]_\gamma // [\bar{1}1\bar{1}]_{\alpha'}$	V18		$[110]_\gamma // [\bar{1}1\bar{1}]_{\alpha'}$
V7	$(1\bar{1}1)_\gamma // (011)_{\alpha'}$	$[10\bar{1}]_\gamma // [\bar{1}\,\bar{1}\,1]_{\alpha'}$	V19	$(11\bar{1})_\gamma // (011)_{\alpha'}$	$[\bar{1}10]_\gamma // [\bar{1}\,\bar{1}\,1]_{\alpha'}$
V8		$[10\bar{1}]_\gamma // [\bar{1}1\bar{1}]_{\alpha'}$	V20		$[\bar{1}10]_\gamma // [\bar{1}1\bar{1}]_{\alpha'}$
V9		$[\bar{1}\,\bar{1}0]_\gamma // [\bar{1}\,\bar{1}\,1]_{\alpha'}$	V21		$[0\bar{1}\,\bar{1}]_\gamma // [\bar{1}\,\bar{1}\,1]_{\alpha'}$
V10		$[\bar{1}\,\bar{1}0]_\gamma // [\bar{1}1\bar{1}]_{\alpha'}$	V22		$[0\bar{1}\,\bar{1}]_\gamma // [\bar{1}1\bar{1}]_{\alpha'}$
V11		$[011]_\gamma // [\bar{1}\,\bar{1}\,1]_{\alpha'}$	V23		$[101]_\gamma // [\bar{1}\,\bar{1}\,1]_{\alpha'}$
V12		$[011]_\gamma // [\bar{1}1\bar{1}]_{\alpha'}$	V24		$[101]_\gamma // [\bar{1}1\bar{1}]_{\alpha'}$

		Habit plane	Plane parallel	Direction parallel	
m_1	m_2	**n** // $[557]_\gamma$	$(111)_\gamma$ // $(011)_{\alpha'}$	$[\bar{1}01]_\gamma$ // $[\bar{1}\,\bar{1}\,1]_{\alpha'}$ (V1)	$[01\bar{1}]_\gamma$ // $[\bar{1}1\bar{1}]_{\alpha'}$ (V4)
14.4	28.6	9.67	0.31	0.76	0.00
17.8	17.8	3.36	0.17	0.64	0.64
28.6	14.4	9.67	0.31	0.00	0.76

K.Iwashita et al. / Table 2

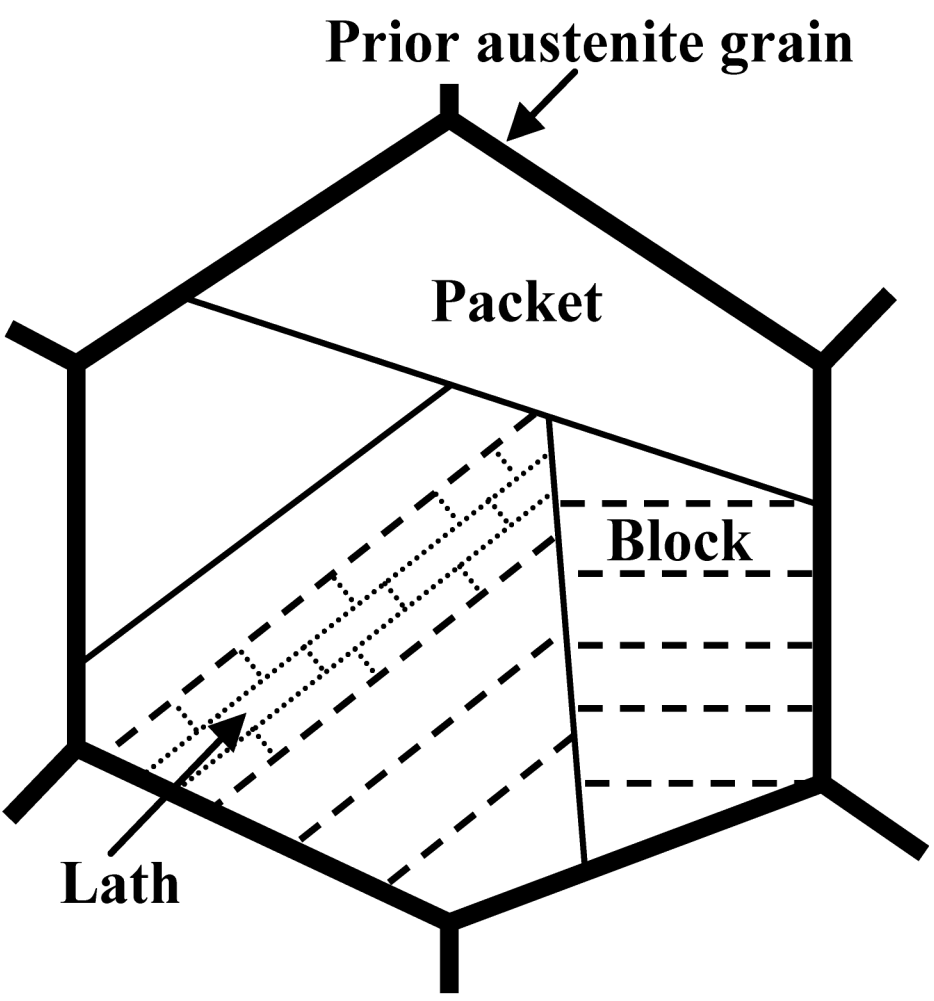

K.Iwashita et al. / Fig.1

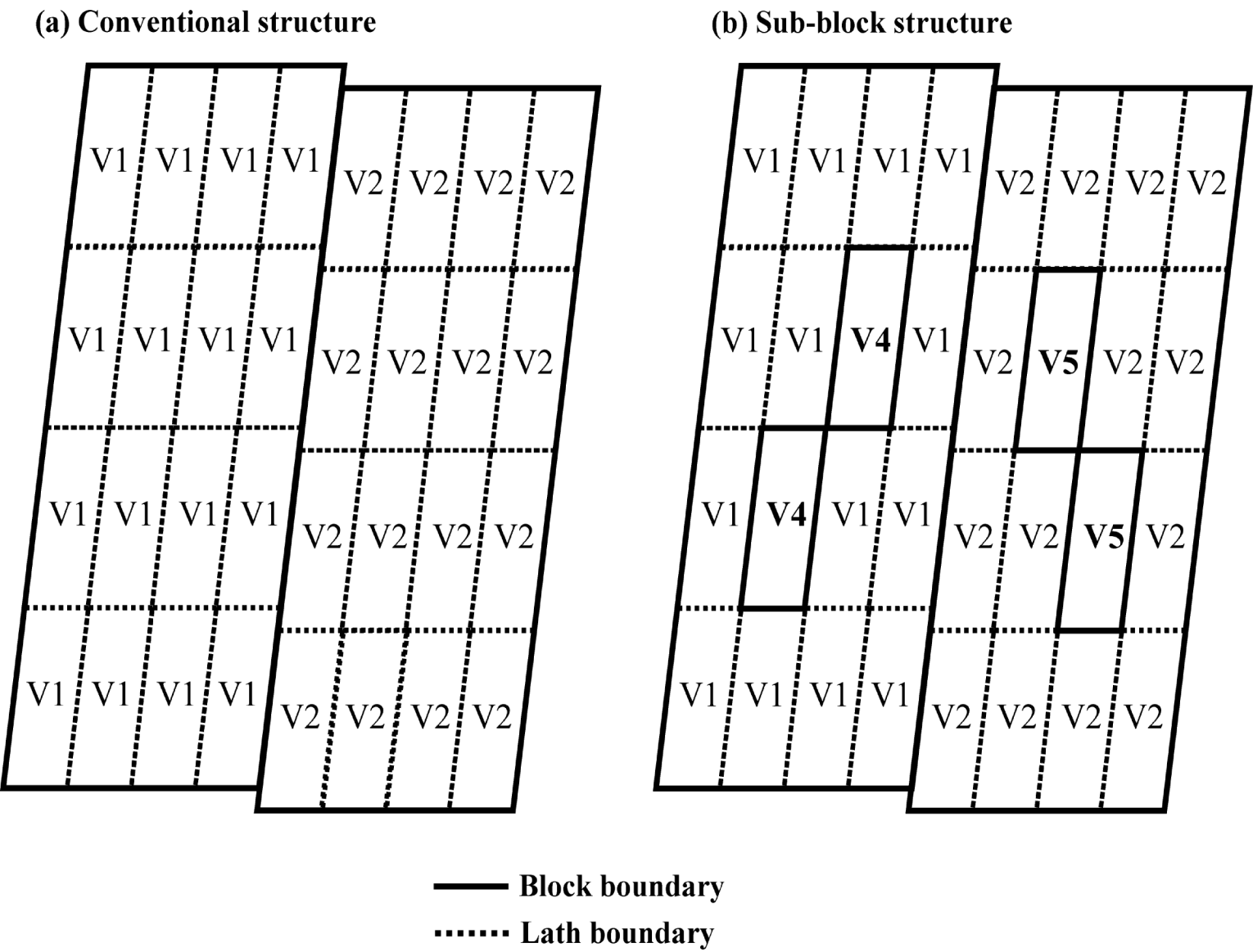

K.Iwashita et al. / Fig.2

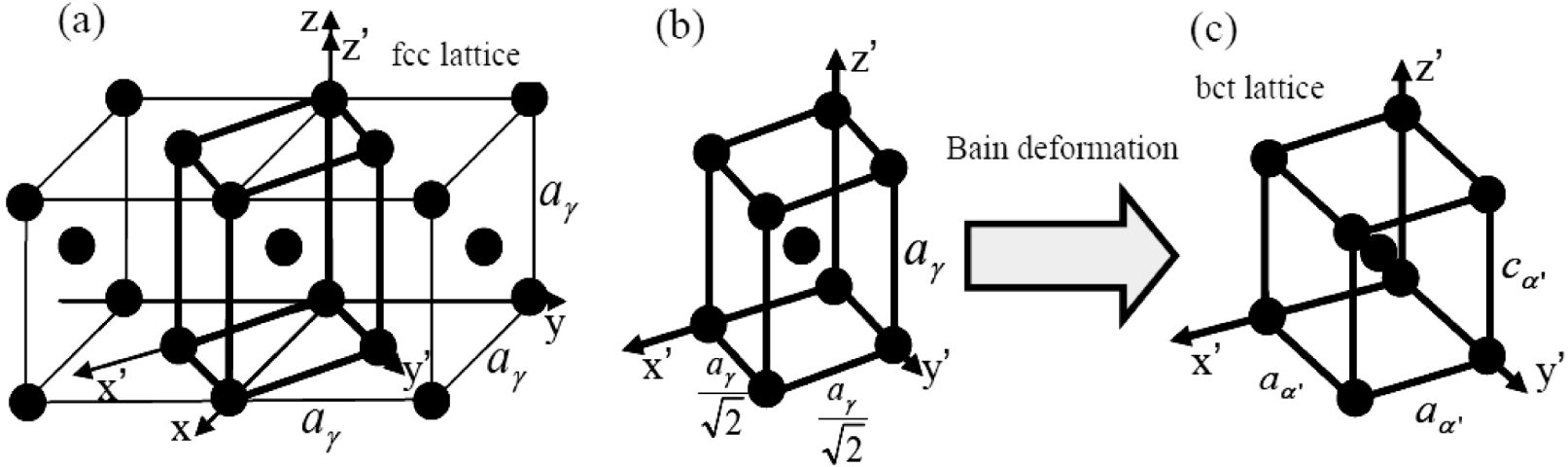

K.Iwashita et al. / Fig.3

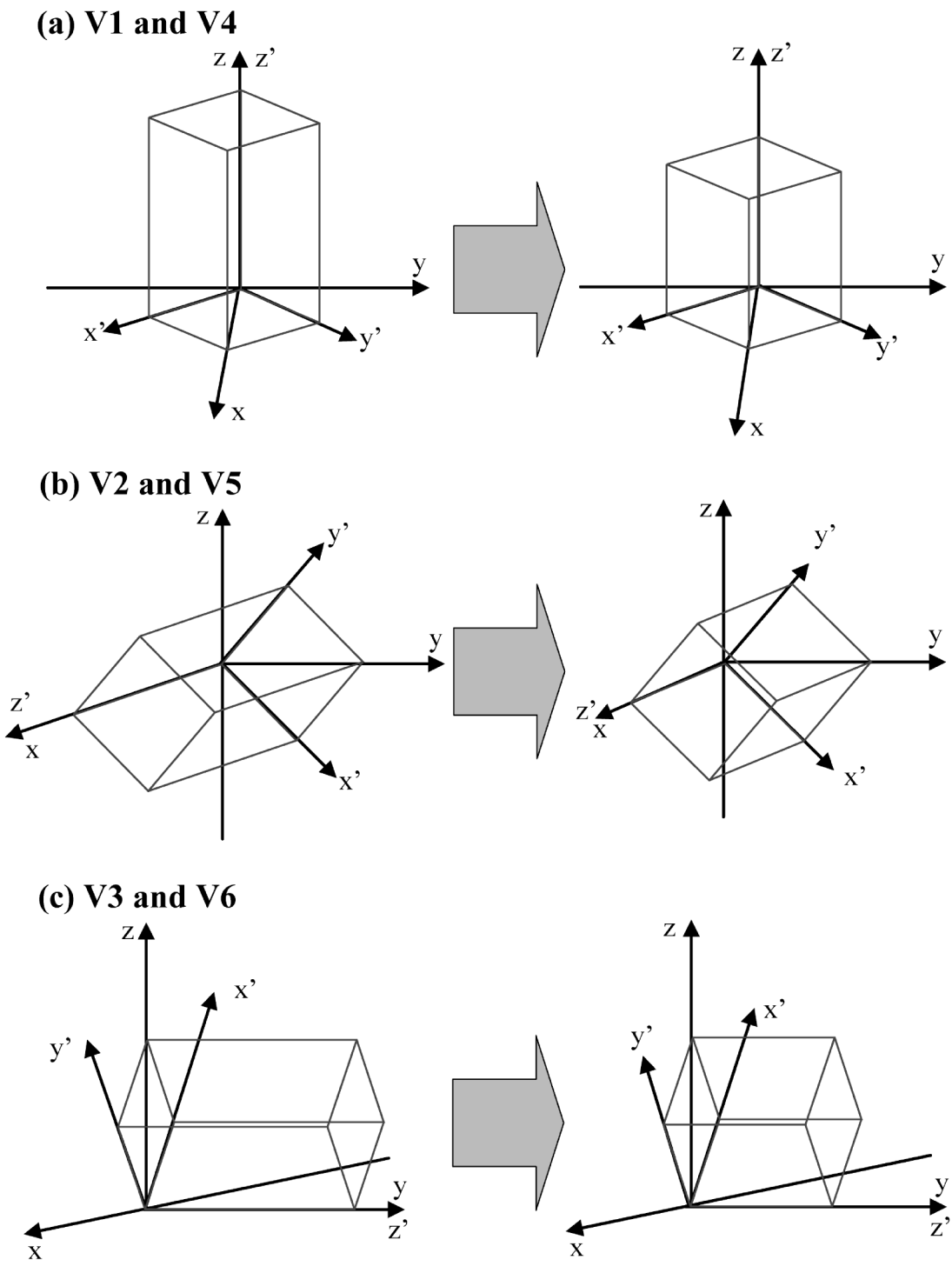

K.Iwashita et al / Fig.4

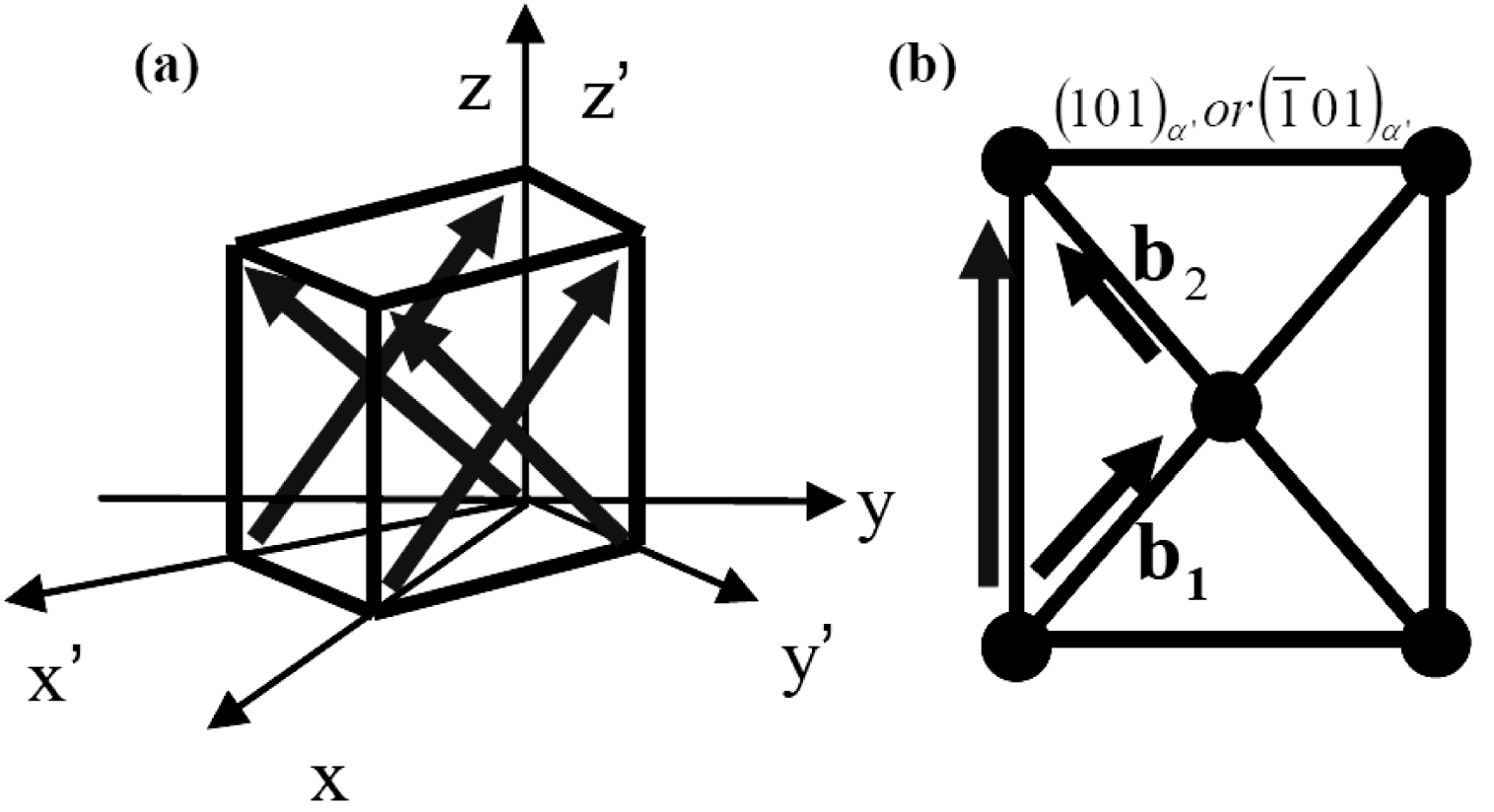

K.Iwashita et al / Fig.5

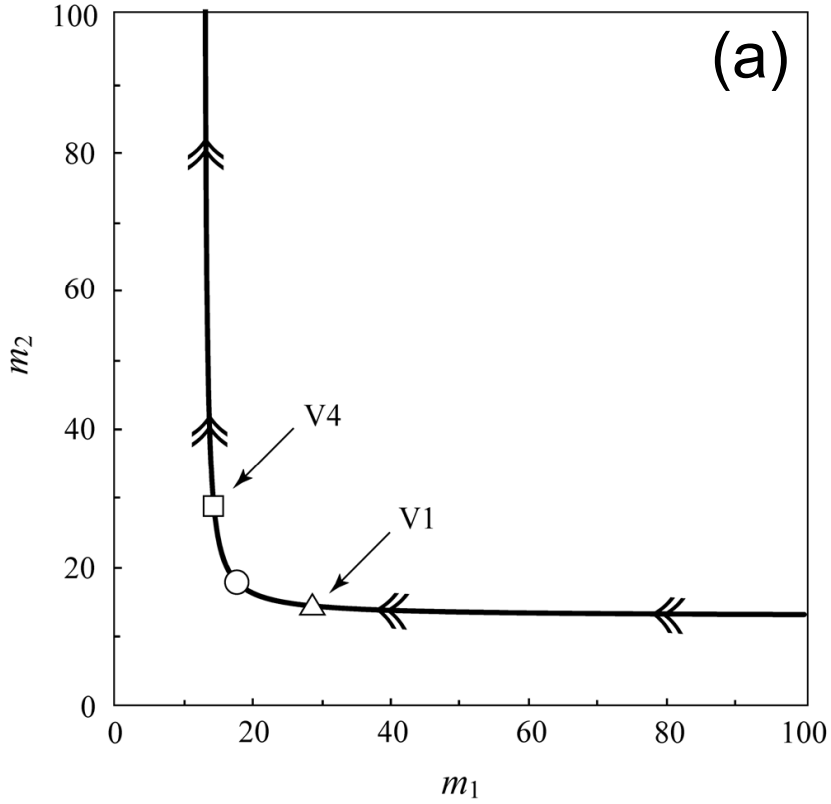

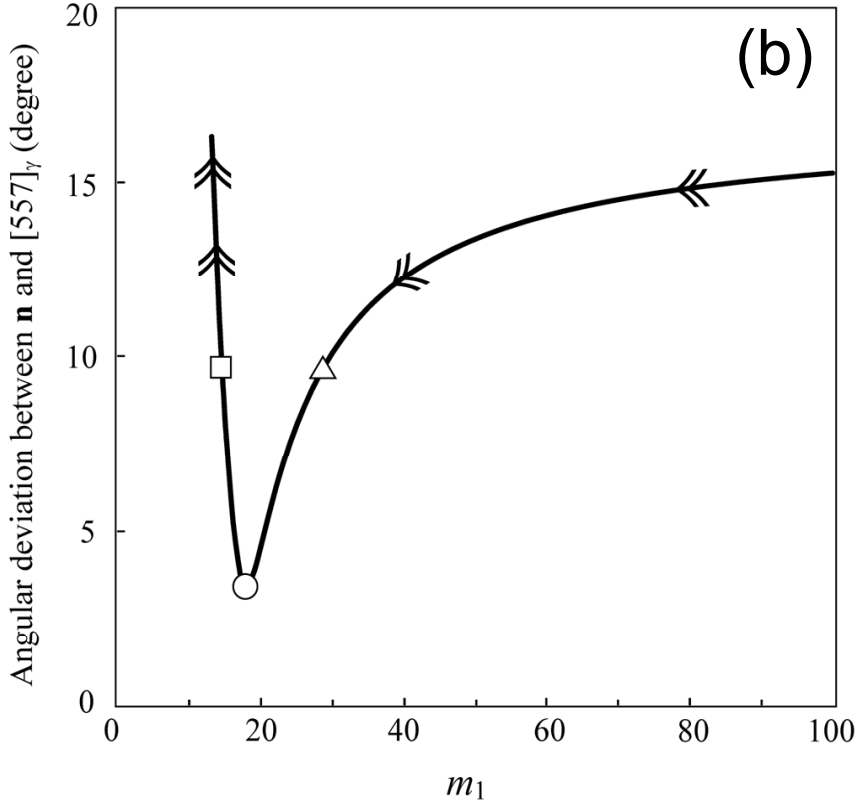

K.Iwashita et al. / Fig.6

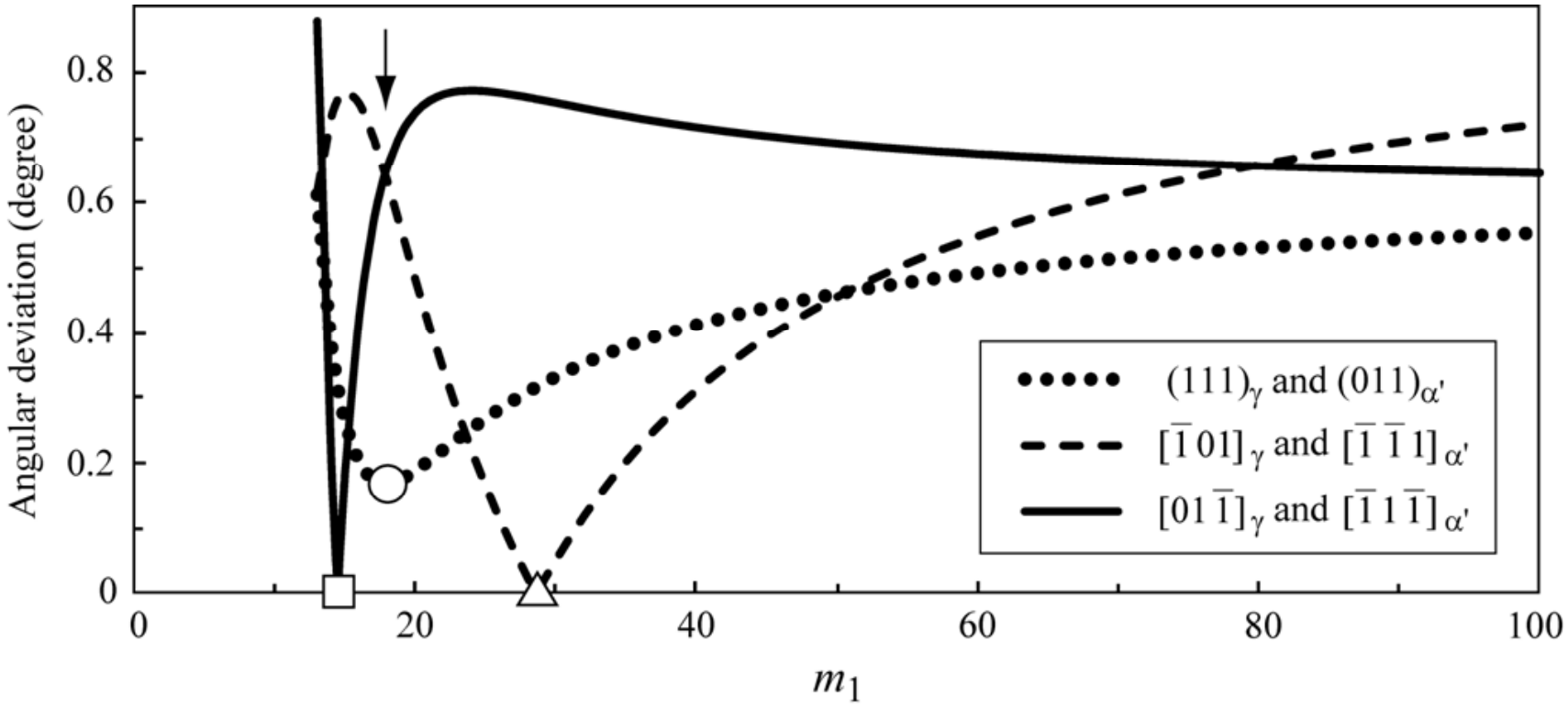

K.Iwashita et al. / Fig.7

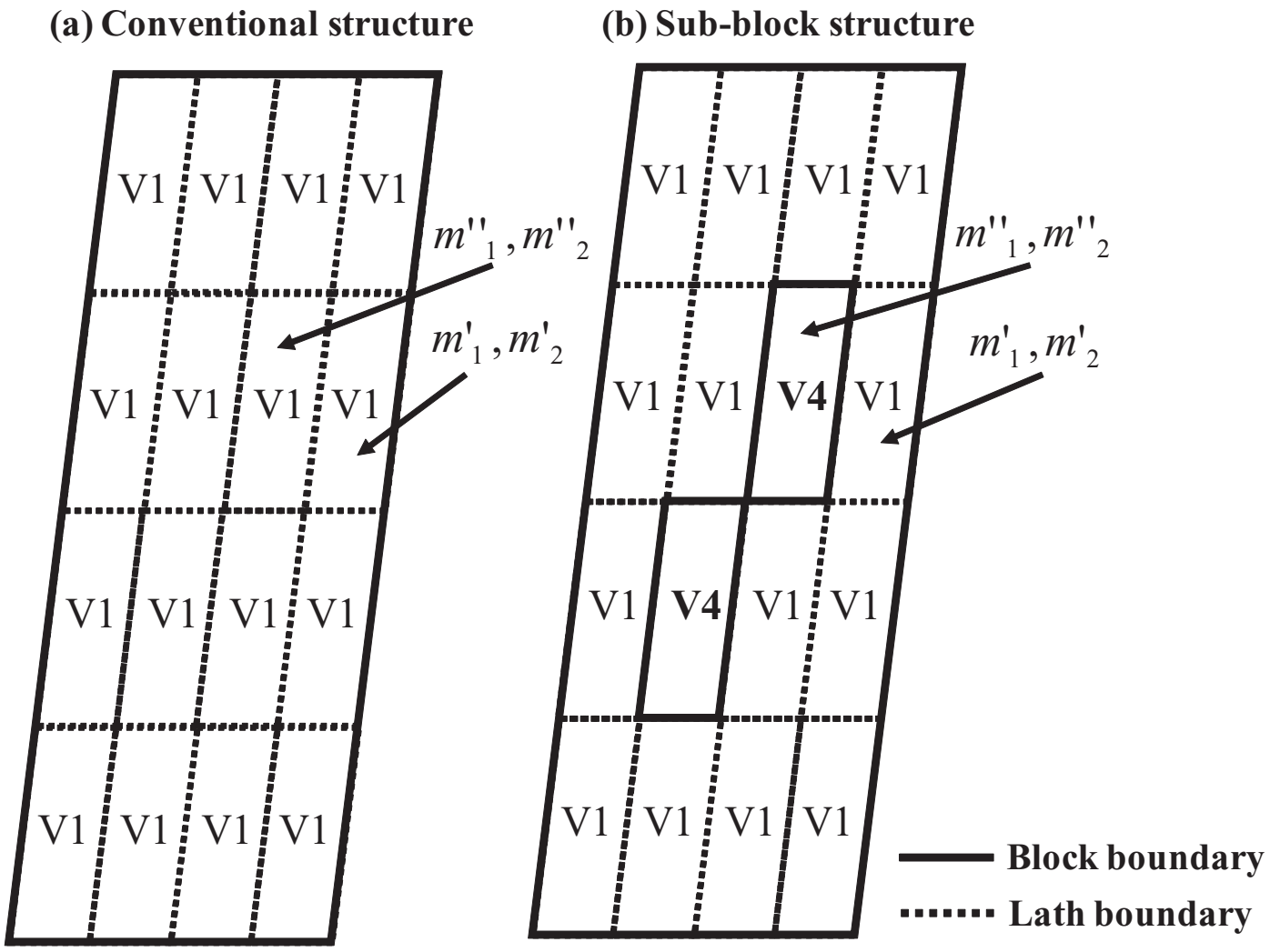

(a) An illustration of a block grain. Here, each lath which belongs to variant 1 has unique m_1 and m_2 values ($m_1 > m_2$). The m values of each lath in this block are slightly different, i.e., $m'_1 \neq m''_1$ and $m'_2 \neq m''_2$.

(b) An illustration of sub-block structure. Each lath has unique m_1 and m_2 values. The m values of each lath in this block are slightly different, same as in (a).
In particular, for the lath that belongs to variant 4, the magnitudes of m_1 and m_2 are alternated, i.e., $m'_1 > m'_2$ and $m''_1 < m''_2$.

K. Iwashita et al. / Fig.8